

## Emission from Dust

Overview of Spectral Energy Distributions (SEDs) in mid- and far-IR

### Far IR (FIR)

warm & cold dust

dust masses

use as star formation (SF) indicator

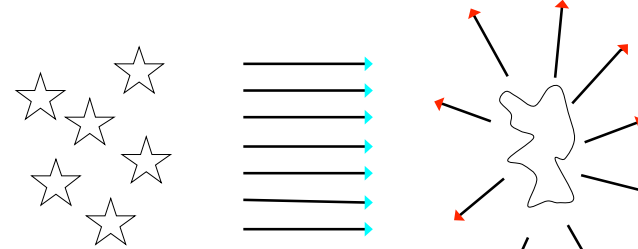
### Mid IR (MIR)

correlation with SF

variation with galaxy type

Extinction implies energy has been absorbed by dust.

Energy is **reprocessed** into the IR.



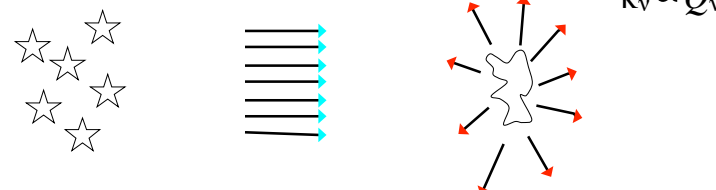
UV & optical light is absorbed by dust...

...which heats up to 10-100K and radiates like a greybody at 10-300μm

2

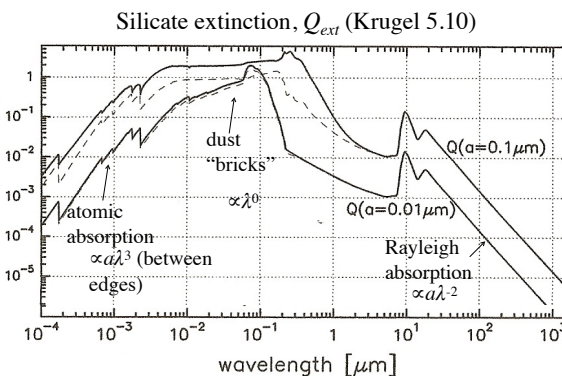
Extinction implies energy has been absorbed by dust.

Dust obeys Kirchoff's Law:  $\epsilon_v = \kappa_v^{abs} B_v(T_d)$



$$\int Q_v^{abs} J_v dv = \int Q_v^{abs} B_v(T_d) dv$$

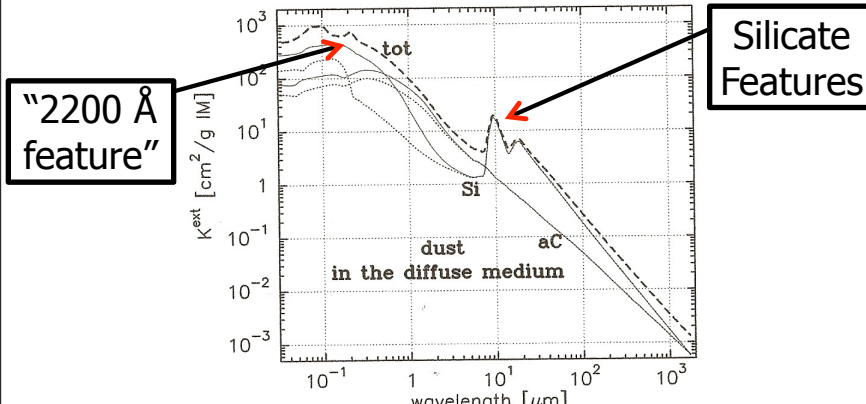
The extinction coefficient  $Q_{ext}$  will vary for different types of dust grains



3

4

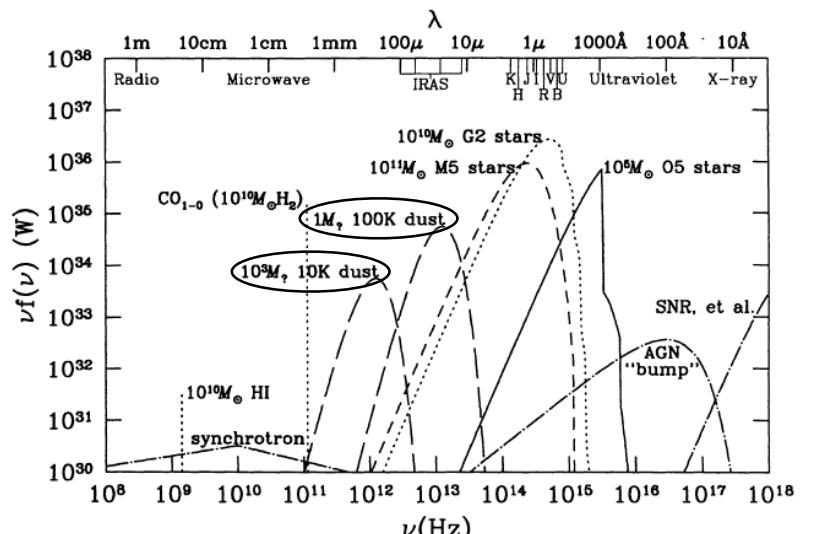
## The total extinction depends on the mixture of dust grains



Total extinction (Krugel Fig. 10.7)

5

## "SED's": Spectral Energy Distributions



7

## Emission from heated dust: Blackbody-ish

Emission from dust grain w/ optical depth  $\tau_\lambda$ :

$$I_\lambda = B_\lambda(T_d)(1 - e^{-\tau_\lambda})$$

At high optical depth:

$$I_\lambda = B_\lambda(T_d)$$

At low optical depth:

$$I_\lambda = \tau_\lambda B_\lambda(T_d) = \kappa_\lambda^{\text{abs}} \sum_d \frac{\epsilon_\lambda}{\kappa_\lambda^{\text{abs}}} = \epsilon_\lambda \Sigma_d$$

Remembering:  $\epsilon_v = \kappa_v^{\text{abs}} B_v(T_d)$

6

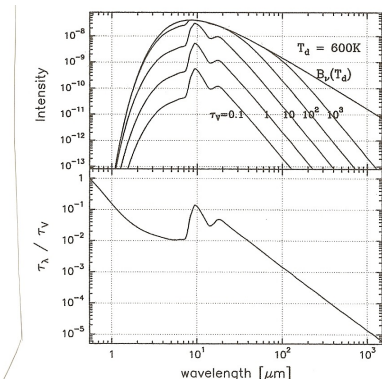
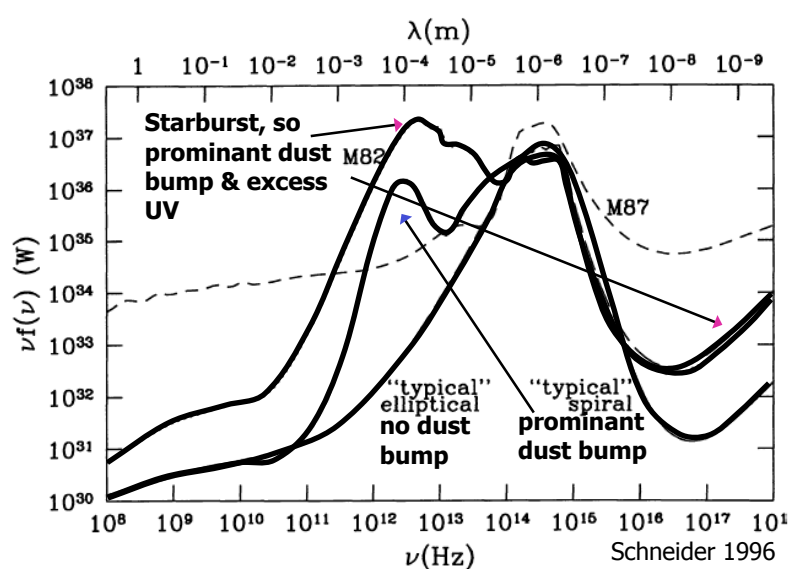


FIGURE 6.4 Bottom: The normalized optical depth of silicate grains with 600Å radius. The wavelength scale starts at 0.55μm where  $\tau_\lambda/\tau_v = 1$ . Top: The intensity (in units  $\text{erg s}^{-1} \text{cm}^{-2} \text{Hz}^{-1} \text{ster}^{-1}$ ) towards a cloud of temperature  $T = 600\text{K}$  filled with such grains for visual optical thickness  $\tau_v$  from 0.1 and 1000.

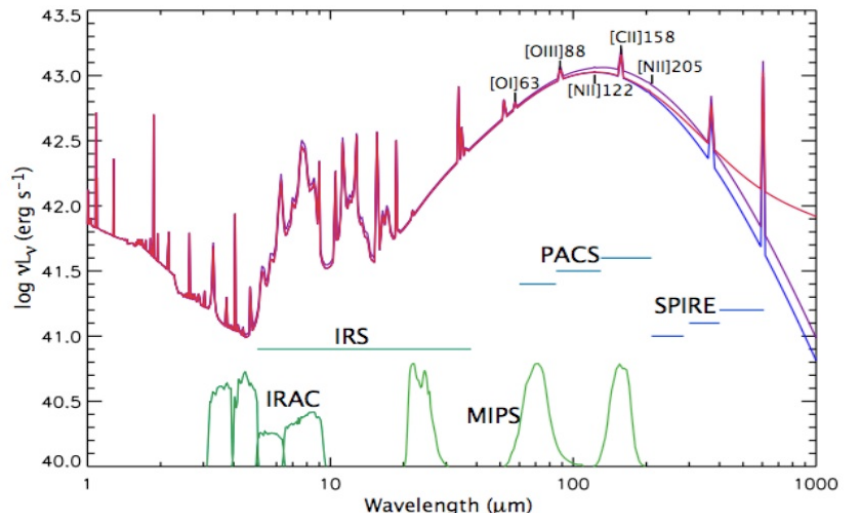
Krugel (2008)



Note:  $\nu f(\nu)$  gives power output, so FIR can dominate the bolometric luminosity

8

## Understanding NIR/MIR/FIR Spectra



## Stars dominate continuum at $\lambda < 3\text{-}4\text{ m}$

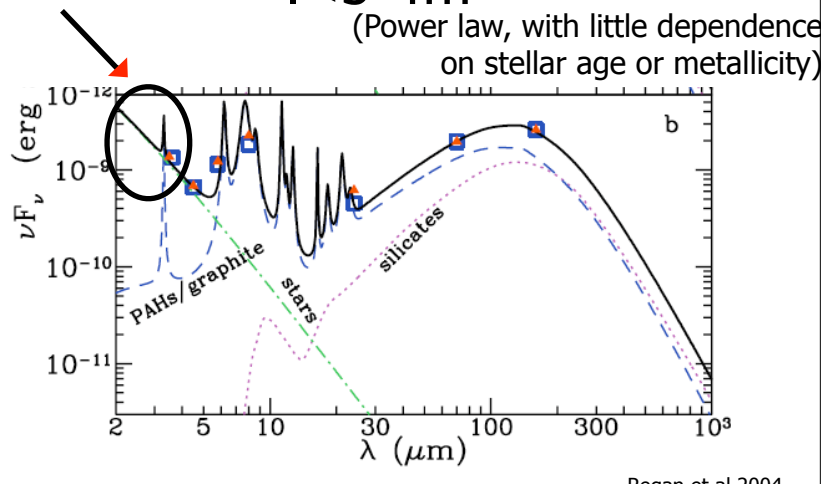
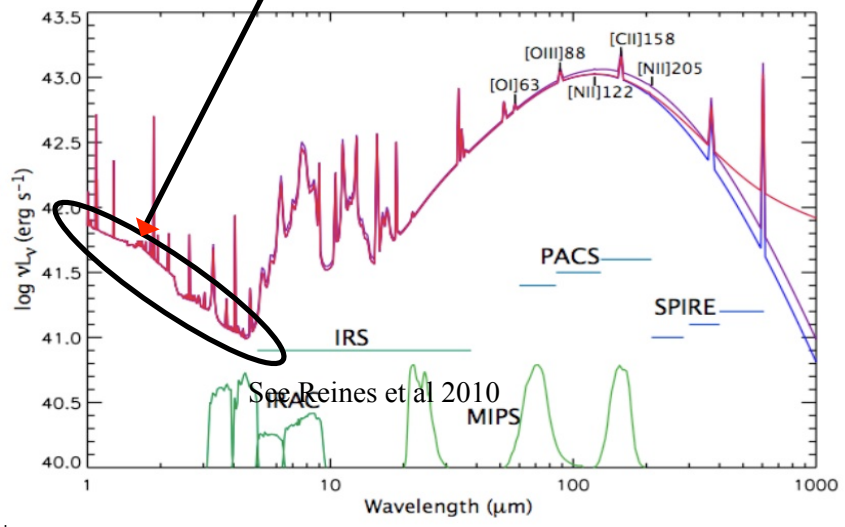
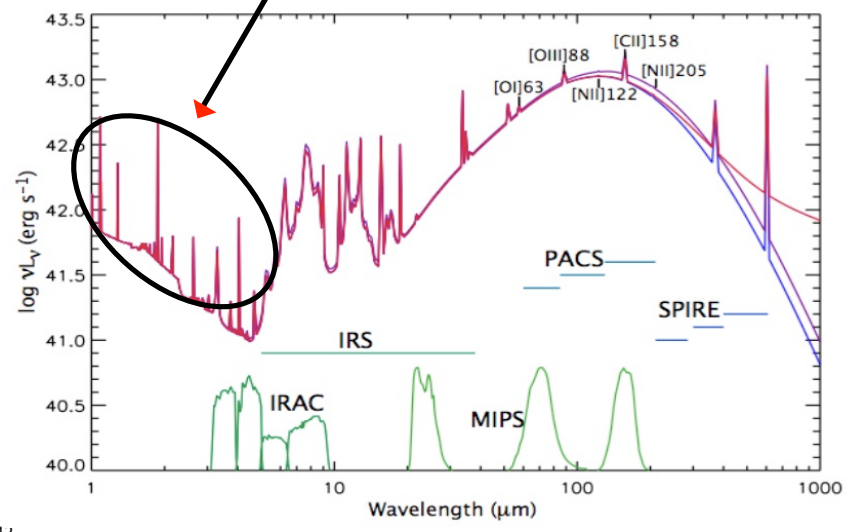


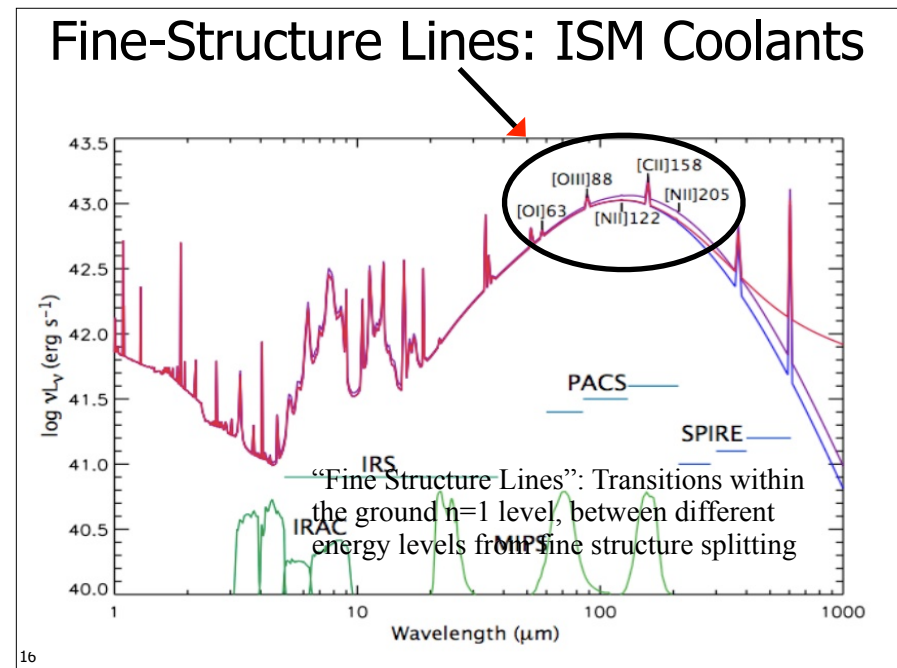
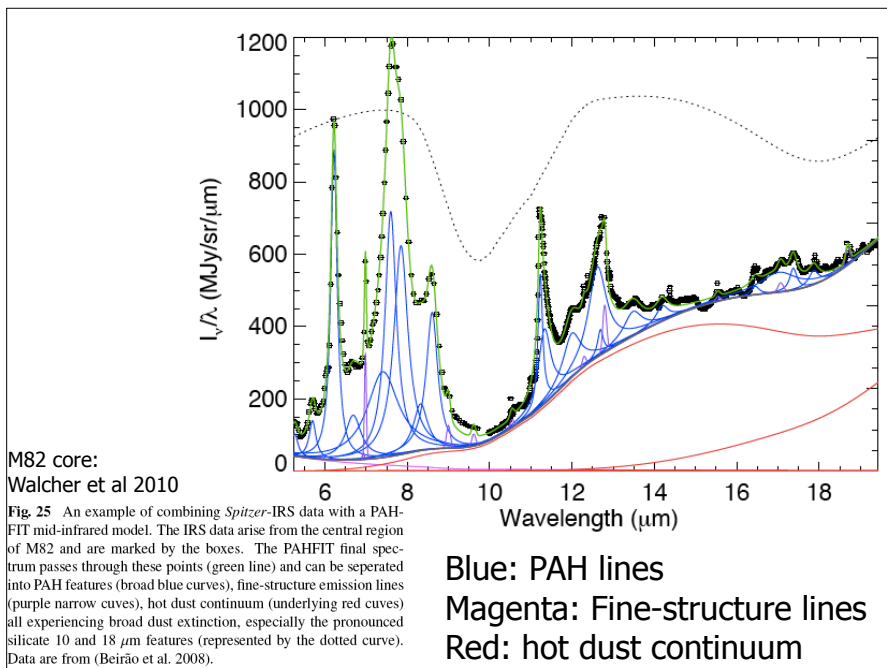
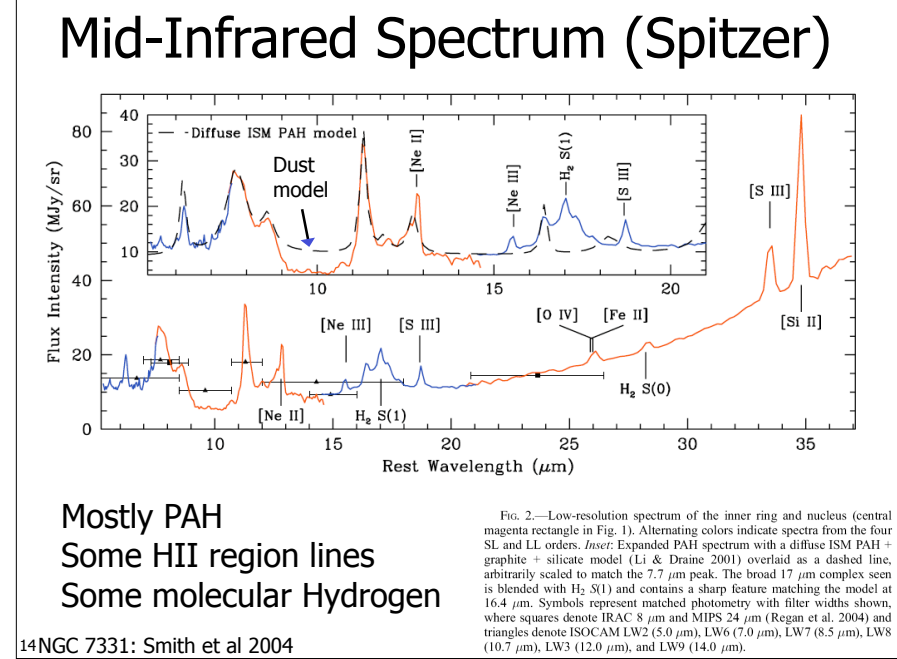
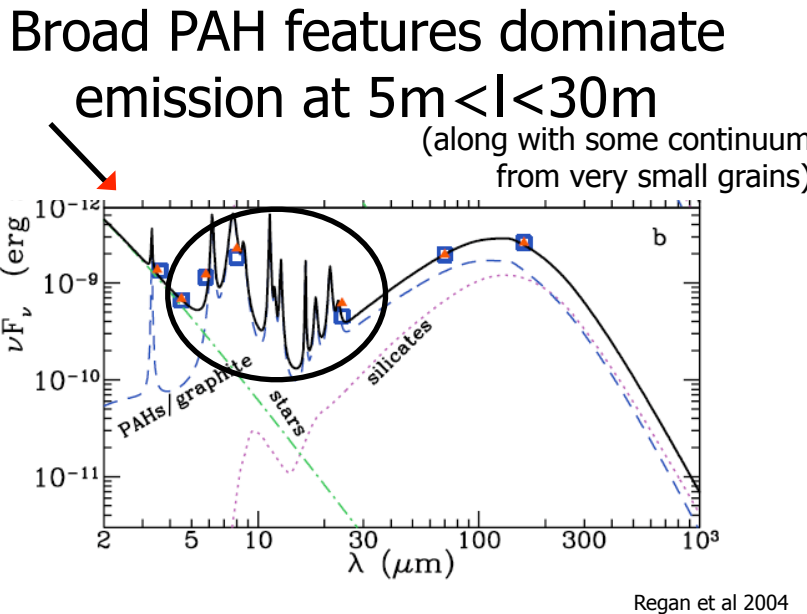
Fig. 3.—SED and model fits to (a) the ring region and (b) the entire galaxy using the model of Li & Draine (2001, 2002b). The solid black lines and red triangles are the model-predicted fluxes, and the blue squares are the observed fluxes. The colored curves indicate the contributions of the different model components.

Note: some additional structure in continuum due to ionized gas

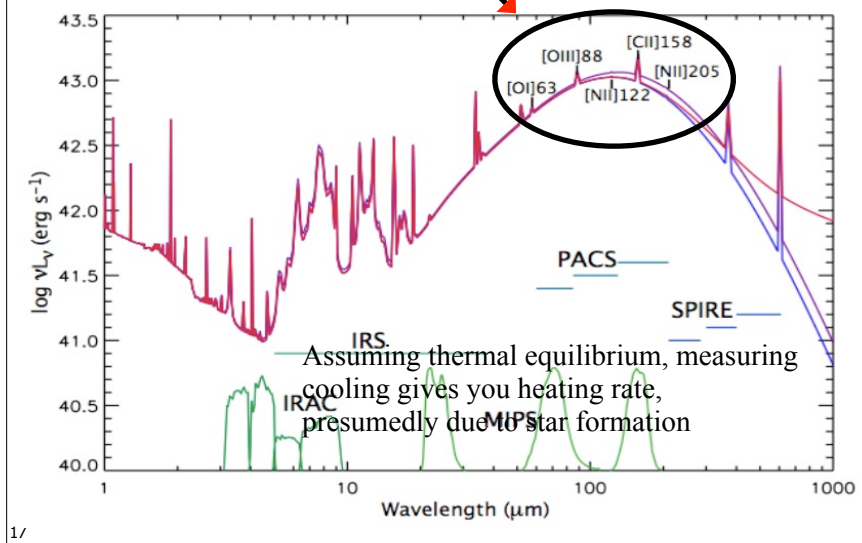


## HII Region Emission Lines (Narrow)





## Fine-Structure Lines: ISM Coolants



## Large grains dominate emission at $\lambda > 30\text{m}$

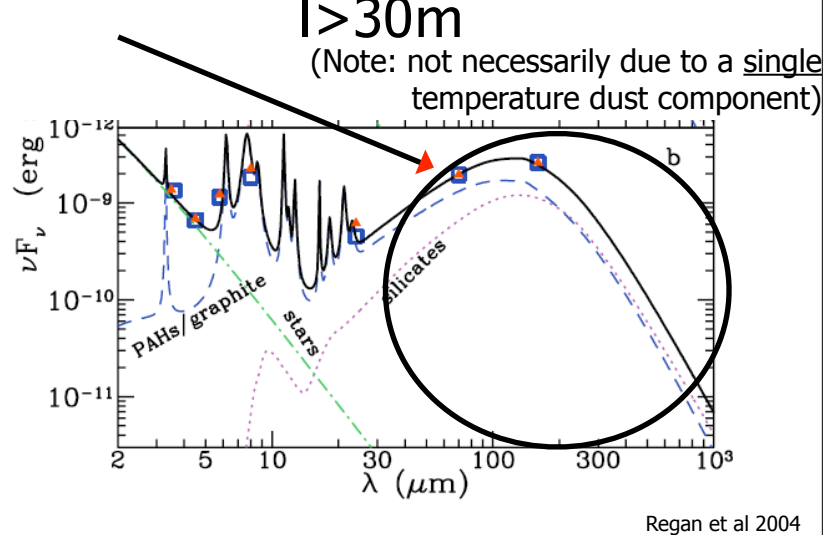
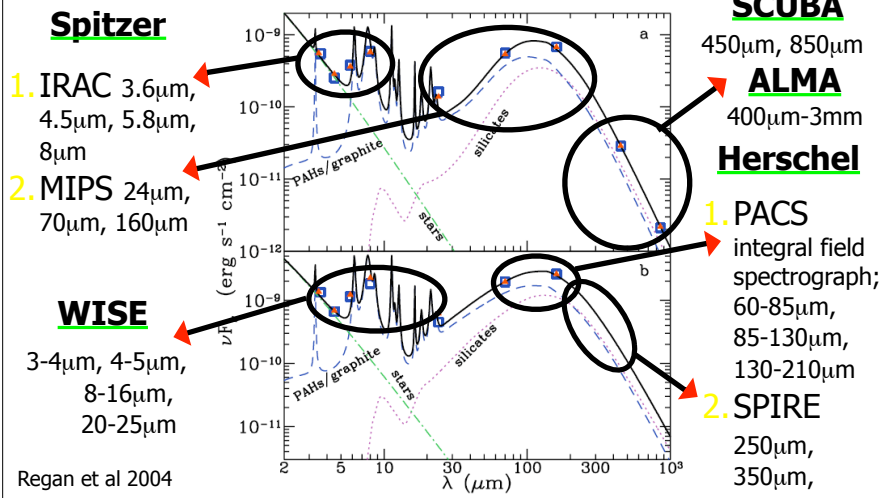


Fig. 3.—SED and model fits to (a) the ring region and (b) the entire galaxy using the model of Li & Draine (2001, 2002b). The solid black lines and red triangles are the model-predicted fluxes, and the blue squares are the observed fluxes. The colored curves indicate the contributions of the different model components.

## MIR/FIR Telescopes (Space, mostly)



## Former State of the Art for MIR/FIR photometry:

**IRAS** (5' beam)  
12μm, 25μm, 60μm, 120μm

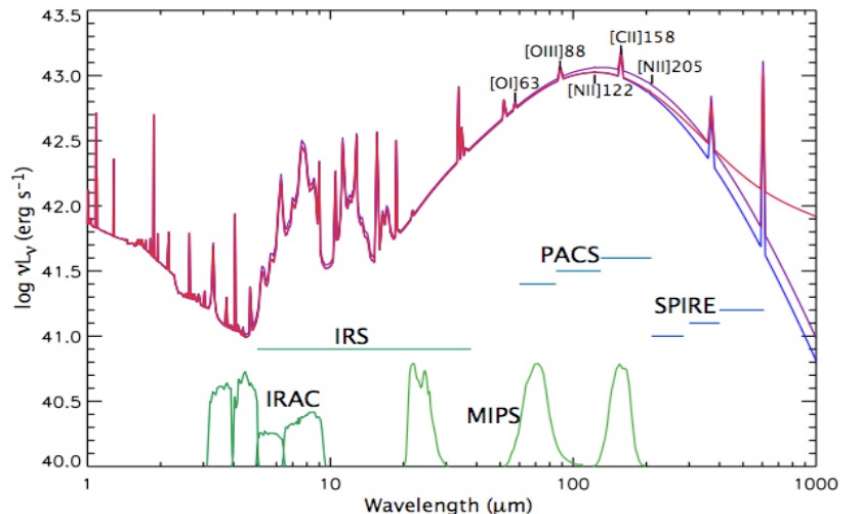
**DIRBE** (0.7° beam)  
1-240μm

**ISO**  
6-12μm (7" beam), 60-170μm (1.3' beam)

Also:

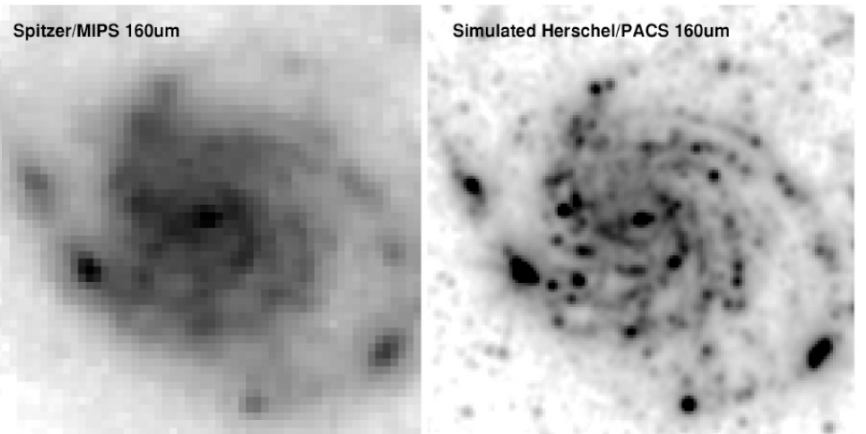
**Planck** (5-10' beam)  
300μm-11,000μm

## Spitzer vs Herschel



<http://www.ast.cam.ac.uk/research/galaxies.and.active.galactic.nuclei/kingfish/science>

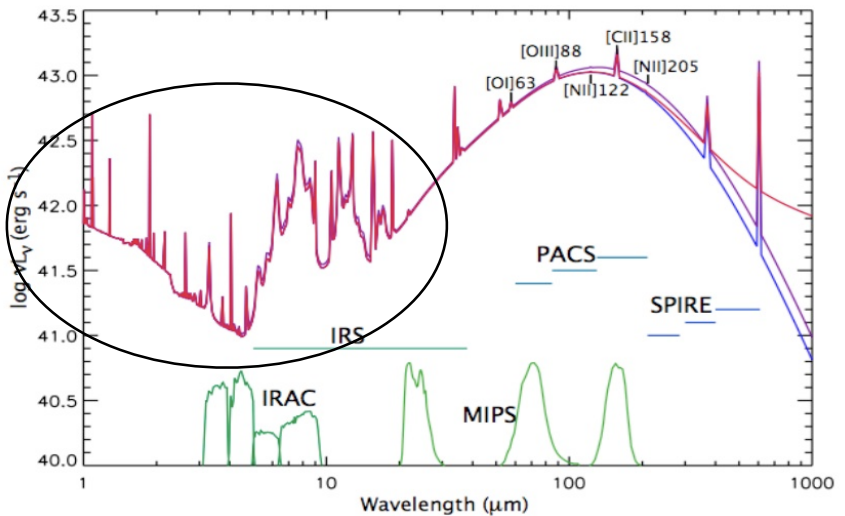
## Spitzer vs Herschel



Much better angular resolution  
(PACS: 5-13'', SPIRE: 18-36'')

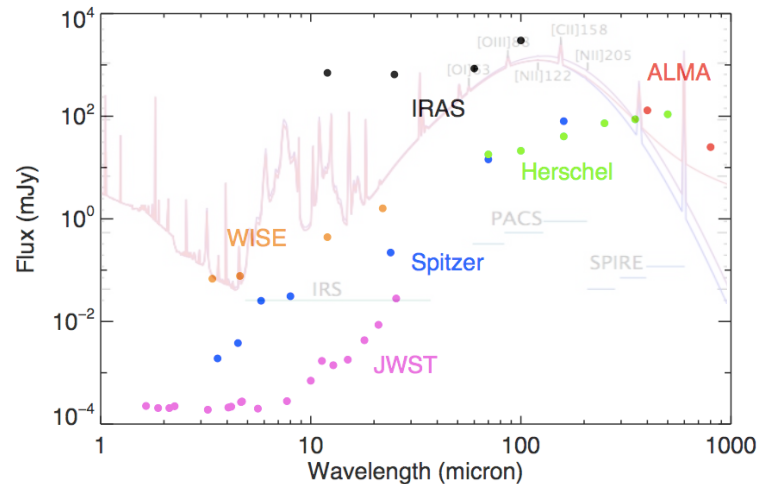
<http://www.ast.cam.ac.uk/research/galaxies.and.active.galactic.nuclei/kingfish/science>

## JWST (2018!)



<http://www.ast.cam.ac.uk/research/galaxies.and.active.galactic.nuclei/kingfish/science>

## Limiting Sensitivities



24

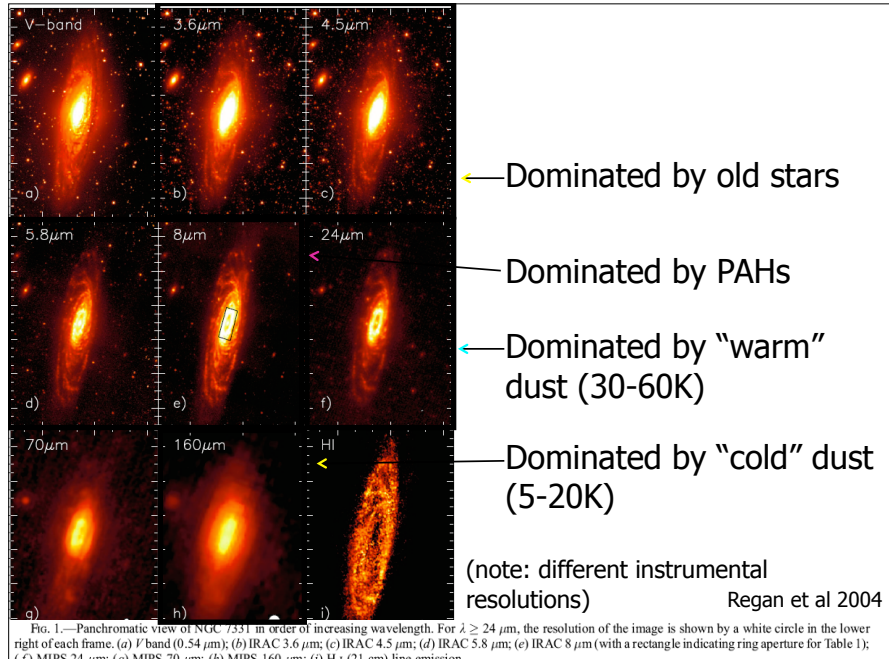


FIG. 1.—Panchromatic view of NGC 7331 in order of increasing wavelength. For  $\lambda \geq 24 \mu\text{m}$ , the resolution of the image is shown by a white circle in the lower right of each frame. (a) V band ( $0.54 \mu\text{m}$ ); (b) IRAC  $3.6 \mu\text{m}$ ; (c) IRAC  $4.5 \mu\text{m}$ ; (d) IRAC  $5.8 \mu\text{m}$ ; (e) IRAC  $8 \mu\text{m}$  (with a rectangle indicating ring aperture for Table 1); (f) MIPS  $24 \mu\text{m}$ ; (g) MIPS  $70 \mu\text{m}$ ; (h) MIPS  $160 \mu\text{m}$ ; (i) H I ( $21 \text{ cm}$ ) line emission.

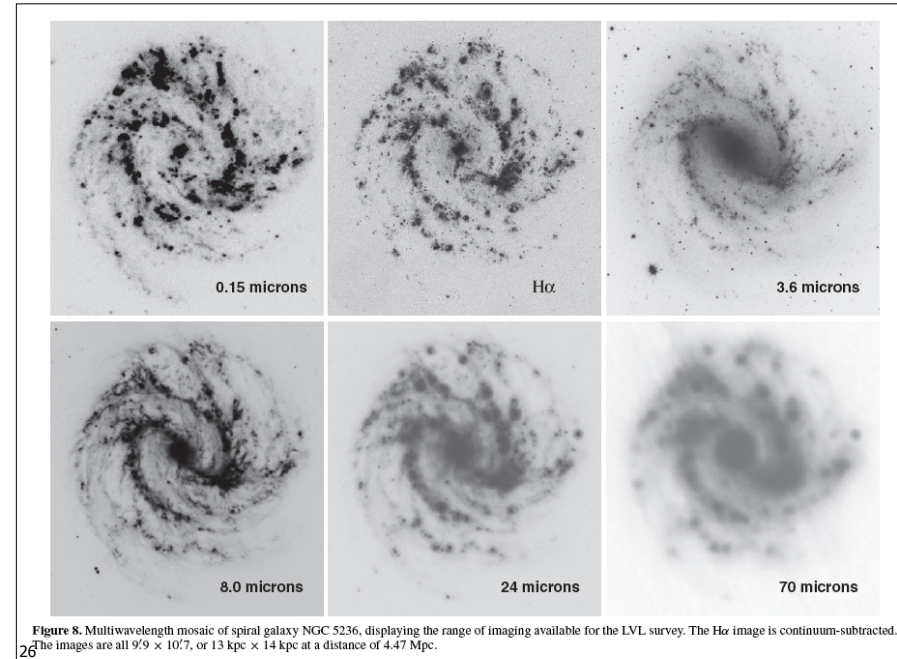
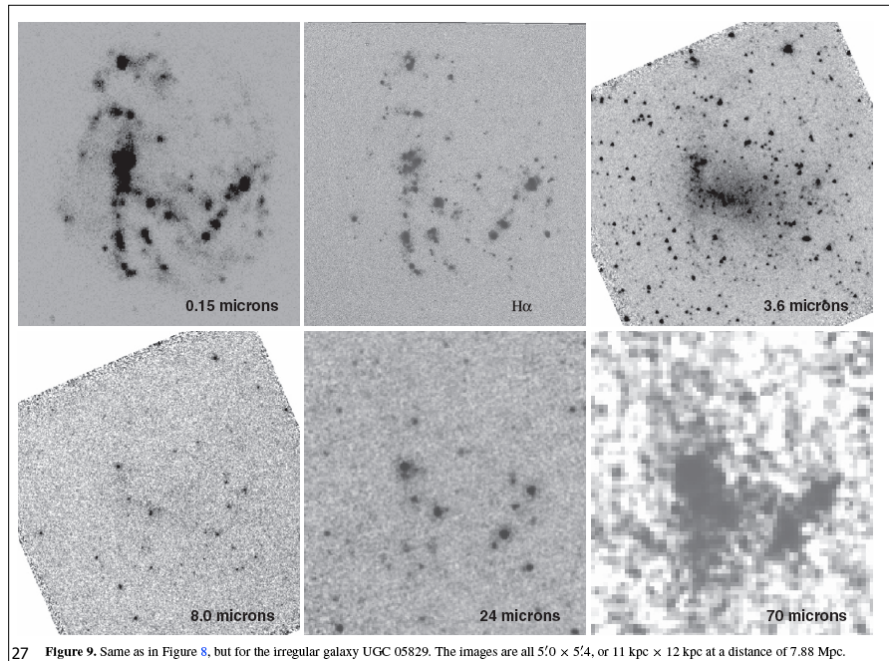


FIGURE 8. Multiwavelength mosaic of spiral galaxy NGC 5236, displaying the range of imaging available for the LVL survey. The H $\alpha$  image is continuum-subtracted. The images are all  $9.9' \times 10.7'$ , or  $13 \text{ kpc} \times 14 \text{ kpc}$  at a distance of  $4.47 \text{ Mpc}$ .  
26



27 Figure 9. Same as in Figure 8, but for the irregular galaxy UGC 05829. The images are all  $5.0' \times 5.4'$ , or  $11 \text{ kpc} \times 12 \text{ kpc}$  at a distance of  $7.88 \text{ Mpc}$ .

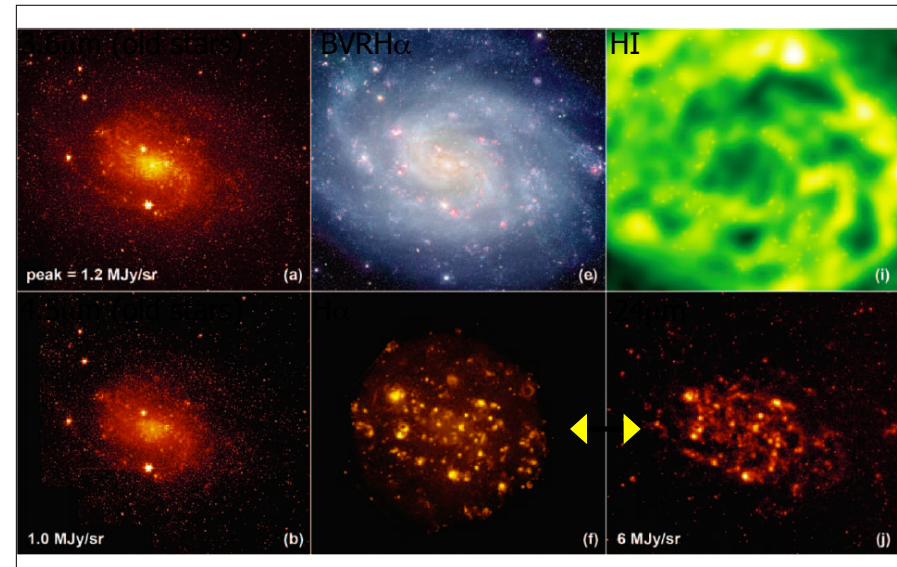
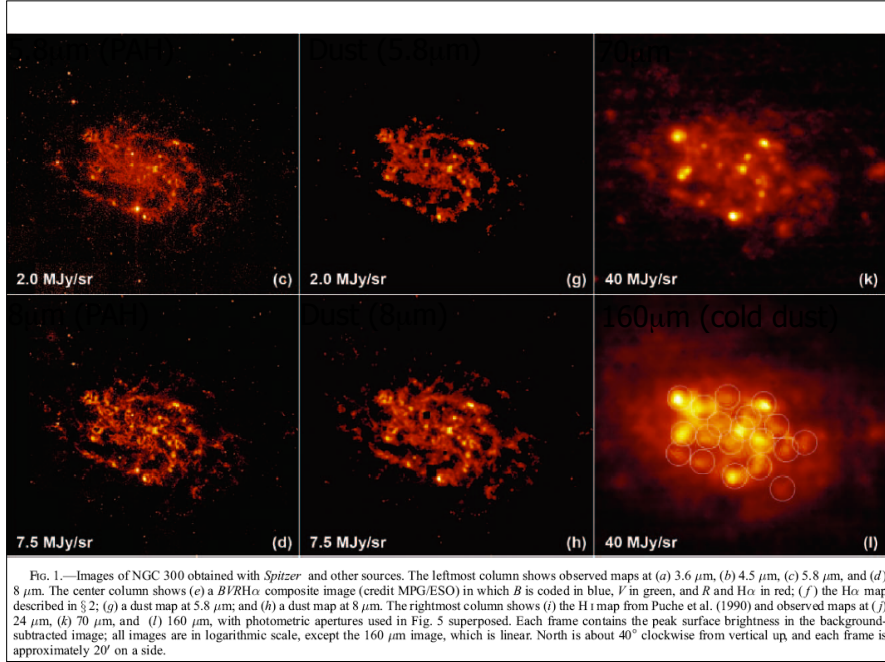


FIG. 1.—Images of NGC 300 obtained with *Spitzer*, and other sources. The leftmost column shows observed maps at (a)  $3.6 \mu\text{m}$ , (b)  $4.5 \mu\text{m}$ , (c)  $5.8 \mu\text{m}$ , and (d)  $8 \mu\text{m}$ . The center column shows (e) a  $BVRH\alpha$  composite image (credit MPG/ESO) in which  $B$  is coded in blue,  $V$  in green, and  $R$  and  $H\alpha$  in red; (f) the  $H\alpha$  map described in § 2; (g) a dust map at  $5.8 \mu\text{m}$ ; and (h) a dust map at  $8 \mu\text{m}$ . The rightmost column shows (i) the HI map from Puche et al. (1990) and observed maps at (j)  $24 \mu\text{m}$ , (k)  $70 \mu\text{m}$ , and (l)  $160 \mu\text{m}$ , with photometric apertures used in Fig. 5 superposed. Each frame contains the peak surface brightness in the background-subtracted image; all images are in logarithmic scale, except the  $160 \mu\text{m}$  image, which is linear. North is about  $40^\circ$  clockwise from vertical up, and each frame is approximately  $20'$  on a side.

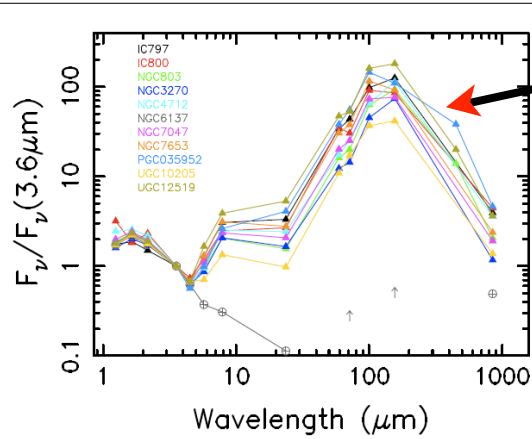
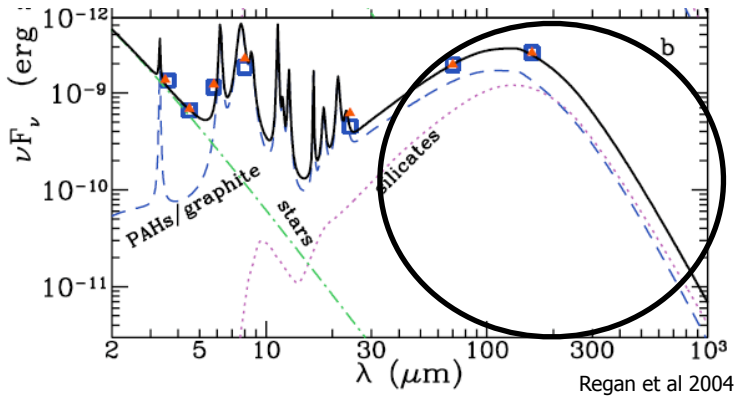


A closer look at:  
FIR-emitting cold dust  
MIR-emitting dust

30

## Cool Dust

Multiple components?  
Constraints on temperature?  
Amount?  
Distribution?



Cool dust is  
a non-  
negligible  
contributor  
to the SED

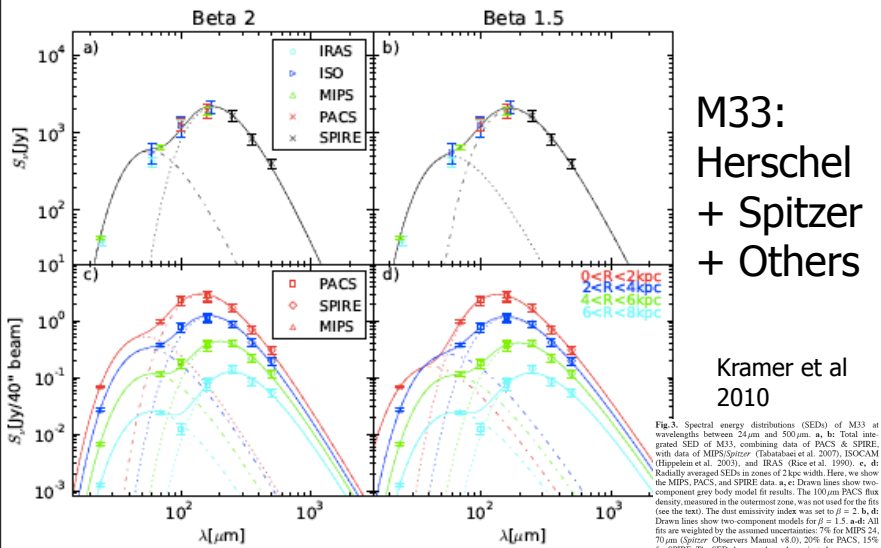
Relatively  
quiescent galaxy  
sample w/  
SCUBA  
observations

"SLUGS"  
Willmer et al 2009

FIG. 2.—Spectral energy distribution for the ensemble of SLUGS galaxies observed for this project, normalized at 3.6  $\mu\text{m}$ . The stellar component shows little variation, while all galaxies, with the exception of NGC 6137 show a bump in the mid-IR due to the aromatic features, followed by a strong peak in the far-IR caused by the presence of cold dust. For NGC 6137 the *Spitzer* measurements at 70 and 160  $\mu\text{m}$  are only upper limits. The combined 24 and 850  $\mu\text{m}$  data points are suggestive of a power-law emission in the mid- and far-IR for this galaxy.

32

## FIR requires warm dust and cold dust



## Cold dust in Orion

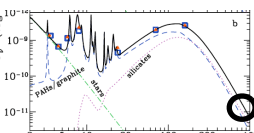
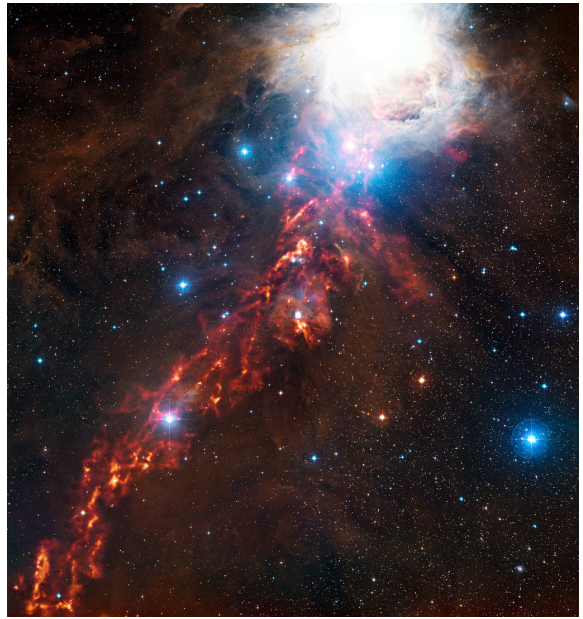


Image by LABOCA (~870mm) on APEX (Atacama Pathfinder Experiment)



34

## Emission is not a perfect blackbody

The new MIPS data combined with existing *IRAS* and SCUBA measurements can be used to estimate the dust component temperatures and masses using composite grey-body curves (e.g., Vlahakis et al. 2005). For two components these are:

$$F_\nu = A_w \nu^\beta B_\nu \left( \frac{\nu}{1+z}, T_w \right) + A_c \nu^\beta B_\nu \left( \frac{\nu}{1+z}, T_c \right) \quad (1)$$

where  $A_w$  and  $A_c$  are the relative contributions due to the warm and cold dust components. The masses can be

Comparing extinction maps to emission suggests “dust emissivity index”  $\beta \sim 1.5 - 2$

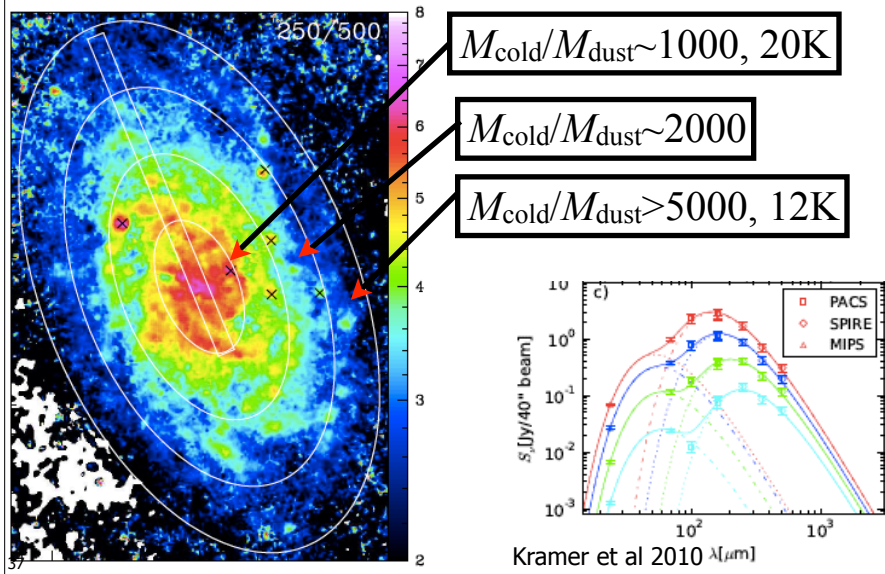
TABLE 5  
TEMPERATURE FIT PARAMETERS FOR SLUGS AND SINGS GALAXIES

Galaxy	T <sub>warm</sub> K	T <sub>cold</sub> K	M <sub>cold</sub> /M <sub>warm</sub>
IC 797	53.9 ± 1.3	18.1 ± 1.0	1213
IC 800	51.1 ± 2.8	16.2 ± 2.8	1065
NGC 3270	56.9 ± 1.9	18.5 ± 0.9	1918
NGC 4712	56.2 ± 0.9	17.0 ± 0.4	3213
NGC 7047	54.5 ± 2.8	18.8 ± 1.4	1248
NGC 7653	54.7 ± 4.0	19.9 ± 2.1	1008
NGC 803	54.7 ± 1.0	18.4 ± 0.4	1812
PGC 035952	54.7 ± 4.4	19.0 ± 2.5	1054
UGC 10205	52.5 ± 2.8	18.4 ± 1.8	1098
UGC 12519	56.0 ± 2.1	19.6 ± 1.0	1054
NGC 337	52.8 ± 3.2	20.6 ± 3.8	337
NGC 1482	56.1 ± 3.6	23.5 ± 5.2	109
NGC 2798	58.0 ± 4.3	24.4 ± 5.4	116
NGC 2976	54.9 ± 3.7	19.1 ± 5.1	800
NGC 3190	54.2 ± 3.4	19.9 ± 3.9	766
Mrk 33	60.7 ± 5.1	24.3 ± 7.2	111
NGC 3521	55.2 ± 2.9	18.5 ± 3.8	985
NGC 3627	55.2 ± 3.0	19.2 ± 4.6	571
NGC 4536	55.5 ± 2.9	20.6 ± 4.6	225
NGC 4569	58.4 ± 3.4	19.7 ± 2.9	973
NGC 4631	52.6 ± 3.4	18.9 ± 4.0	539
NGC 4826	52.4 ± 3.8	20.3 ± 5.0	362
NGC 5195	59.4 ± 27.9	25.7 ± 9.5	258
NGC 5713	54.9 ± 2.9	20.2 ± 4.1	307
NGC 5866	57.2 ± 16.1	24.5 ± 3.1	878
NGC 7331	54.4 ± 3.2	19.4 ± 2.8	660

Most dust mass is in the cold ( $T < 20\text{K}$ ) component

35

## Cold component varies radially



## Inferred dust-to-gas ratios

Based on SED modeling

Much larger than 1st generation fits which lacked constraints on cold dust

Metallicity-dependent, as expected

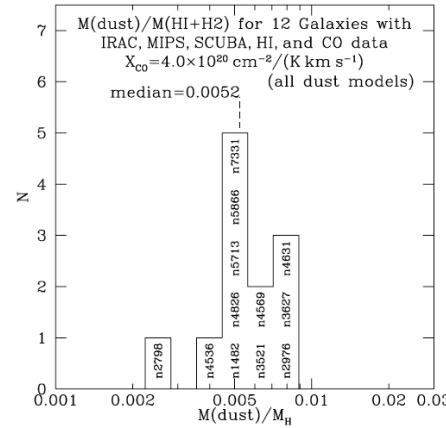


FIG. 4.—Histograms of  $M_{\text{dust}}/M(\text{H}_1 + \text{H}_2)$  for the 12 galaxies in the sample for which both  $\text{H}_1$  21 cm and CO 1–0 have been measured, using  $X_{\text{CO}} = 4 \times 10^{20} \text{ cm}^{-2} (\text{K km s}^{-1})^{-1}$  to estimate  $M(\text{H}_2)$ .

Draine et al 2007; SINGS data

38

## Derived from SED fits to dust models

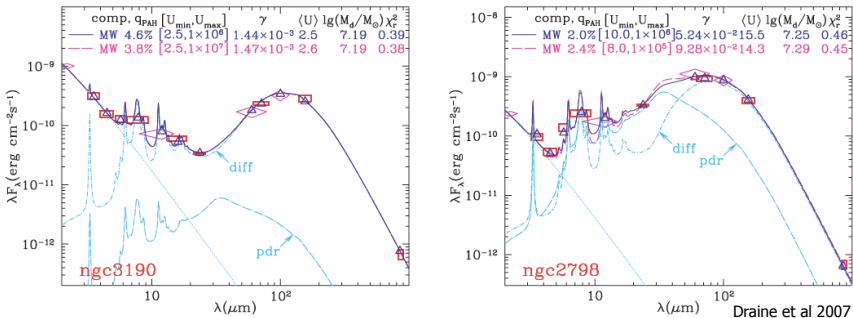


FIG. 3.—(a) SED for the SAap galaxy NGC 3190. Rectangles show observed fluxes in the IRAC, MIPS, SCUBA, and IRS 16  $\mu\text{m}$  bands; diamonds show 2MASS 2.2  $\mu\text{m}$  and IRAS 12, 60, and 100  $\mu\text{m}$  fluxes. Vertical extent of rectangles and diamonds corresponds to  $\pm 1$  range, and width corresponds to nominal width of band. The solid line shows the best-fit  $U_{\text{max}} = 10^6$  model, with IRAC, MIPS, IRS 16  $\mu\text{m}$ , IRAS, and SCUBA data used to constrain the fit;  $N_b = 12$  for NGC 3190. Triangles show the model convolved with the IRAC, MIPS, IRS 16  $\mu\text{m}$ , IRAS, and SCUBA bands. Dot-dashed lines show separate contributions of starlight and emission from dust heated by  $U = U_{\text{max}}$  (labeled “diff”) and dust heated by  $U_{\text{min}} < U < U_{\text{max}}$  (labeled “pdr”). The long-dashed line shows the best-fit model when  $U_{\text{max}}$  is unconstrained; for this case the model spectrum is nearly indistinguishable for the simple reason that there is relatively little dust ( $\gamma \approx 0.0015$ ), and therefore relatively little power, in the “pdr” component. (b) Same as (a), but for the SBA galaxy NGC 2798, with  $N_b = 11$  (global imaging in the IRS 16  $\mu\text{m}$  band is unavailable).

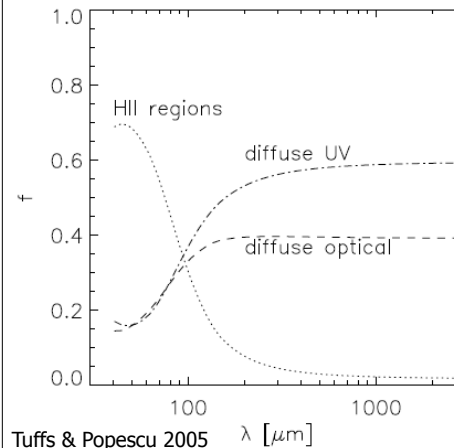
“Diffuse” dust, heated by low intensity background radiation field within the galaxy

39 “PDR” dust, heated in high-intensity radiation field

## What heats the dust?

Warm Dust:  
HII regions

Cool/Cold Dust:  
Diffuse ISRF

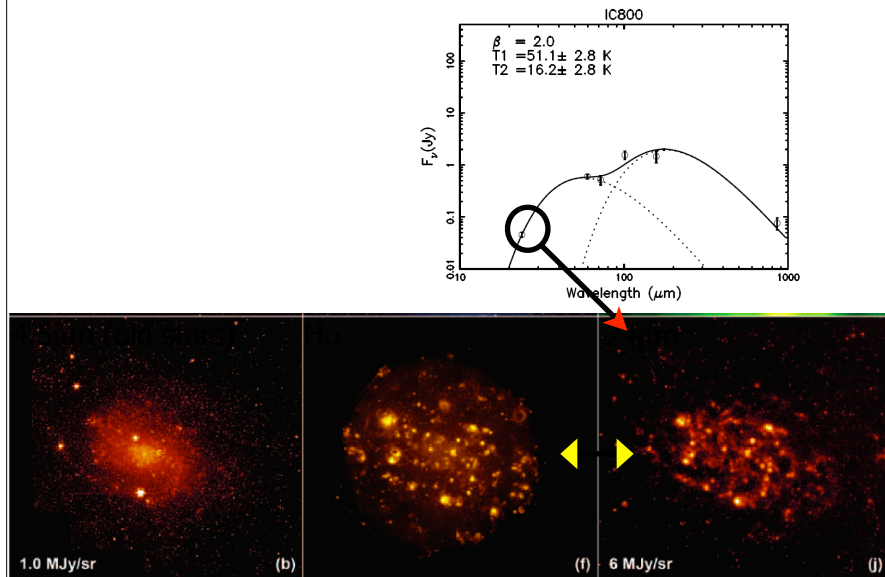


ISRF=Insterstellar Radiation Field

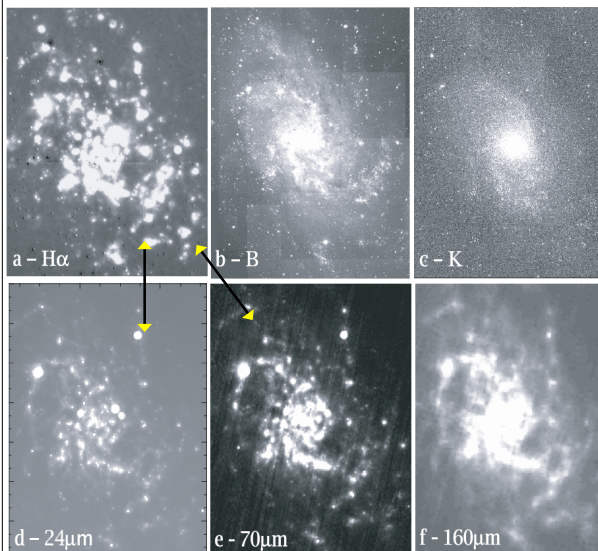
FIGURE 9. Left: The radial profile of NGC 891 at 170  $\mu\text{m}$  (Popescu et al. [71]) produced by integrated the emission parallel to the minor axis of the galaxy for each bin along the major axis. Solid line: model prediction; diamonds: observed profile; dotted line: beam profile. Right: The fractional contribution of the

4 three stellar components to the FIR emission of NGC 891 (Popescu et al. [65]).

Visually, hot dust is distributed like H $\alpha$



Hinz et al 2004



24 $\mu$  & 70 $\mu$   
probably  
heated by  
same  
mechanism  
as ionizes H $\alpha$

24 $\mu$ m  
adopted as  
a star  
formation  
indicator

FIG. 3.—Images of M33 at (a) H $\alpha$ , (b) B band, (c) K band, (d) 24  $\mu$ m, (e) 70  $\mu$ m, and (f) 160  $\mu$ m. The H $\alpha$  and 24  $\mu$ m data have been convolved to the 70  $\mu$ m resolution of 18''. The field of view is approximately 38''  $\times$  44''. North is up, and east is to the left.

MIR-Emitting Dust

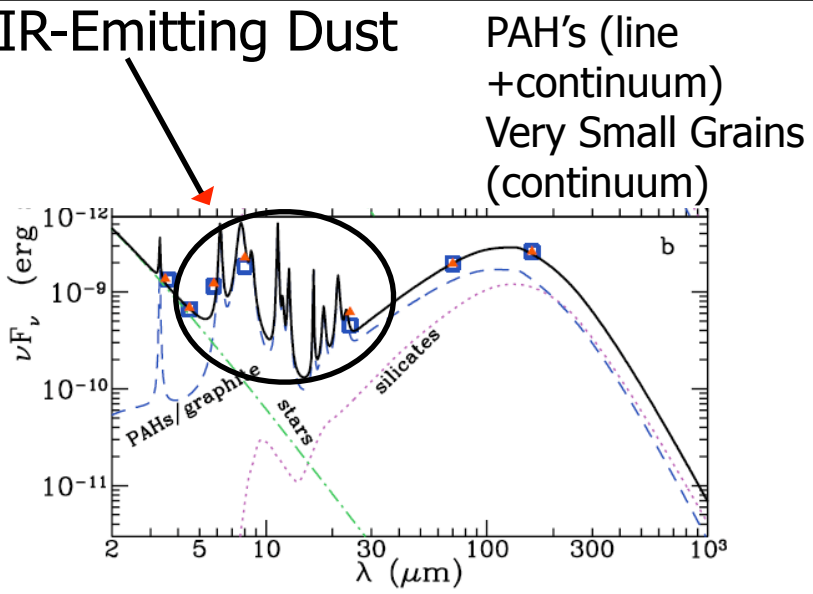


Fig. 3.—SED and model fits to (a) the ring region and (b) the entire galaxy using the model of Li & Draine (2001, 2002b). The solid black lines and red triangles are the model-predicted fluxes, and the blue squares are the observed fluxes. The colored curves indicate the contributions of the different model components.

PAH's (line  
+continuum)  
Very Small Grains  
(continuum)

Why not a black body for small grains?

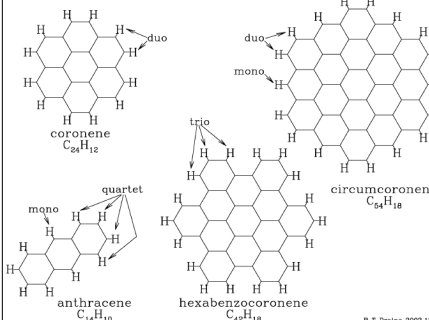


Figure 7. The structure of 4 PAH molecules. Examples of mono, duo, trio, and quartet H sites are indicated.

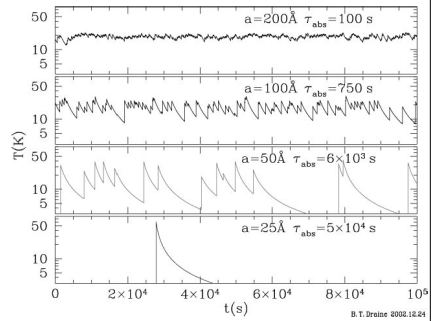
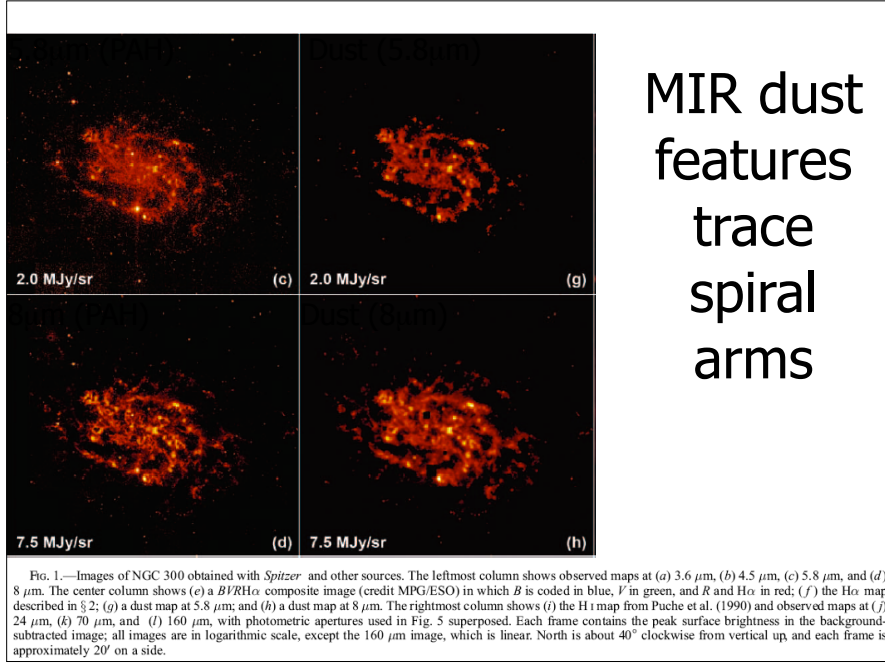


Figure 13 A day in the life of four carbonaceous grains, heated by the local interstellar radiation field.  $\tau_{\text{abs}}$  is the mean time between photon absorptions (Draine & Li 2001).

Small enough that quantum mechanical  
molecular effects are important  
Heating can be stochastic when cooling is rapid



## 2. Ellipticals lack significant MIR emission

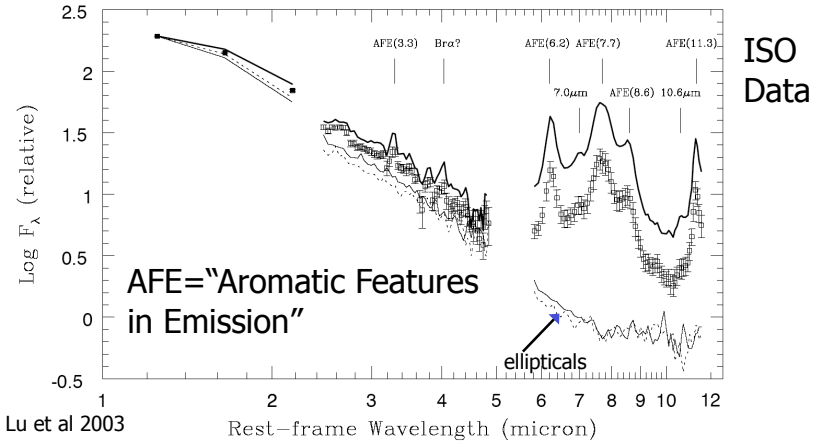
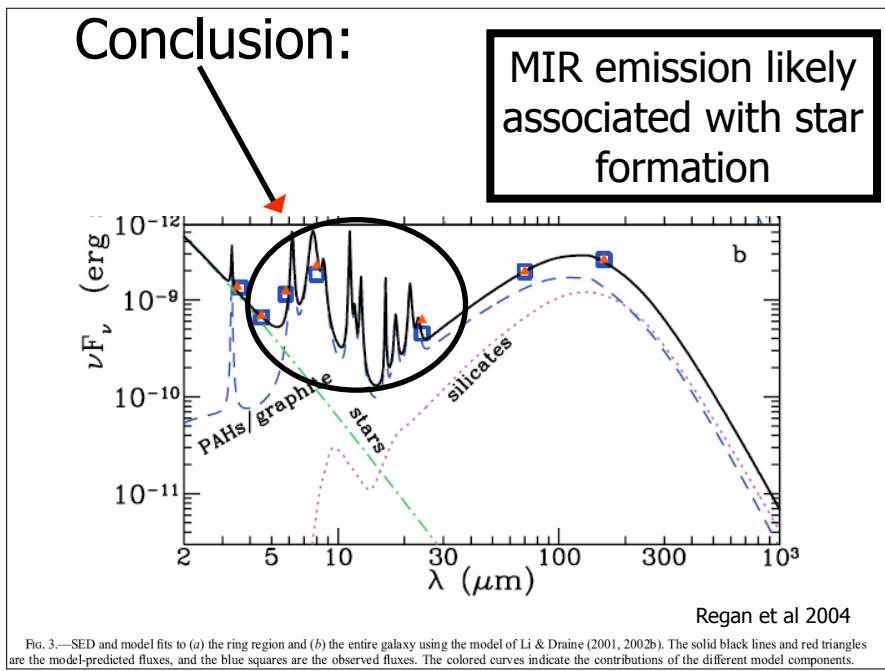


FIG. 3.—Plot of the average rest-frame spectra derived from weighted averages of the spectra of 40 galaxies (see § 3.1). The squares represent the average spectrum obtained by normalizing to the  $J$  fluxes, while the thick solid curve results from normalizing by the integrated flux of AFE (7.7  $\mu\text{m}$ ). Representative error bars are shown only for the former; note that the error bars should be smallest near the fiducial wavelength used for the normalization. The spectra of two elliptical galaxies are also shown: NGC 3379 (thin solid curve) and NGC 4374 (dotted line).



Low luminosity galaxies tend to be missing PAH's

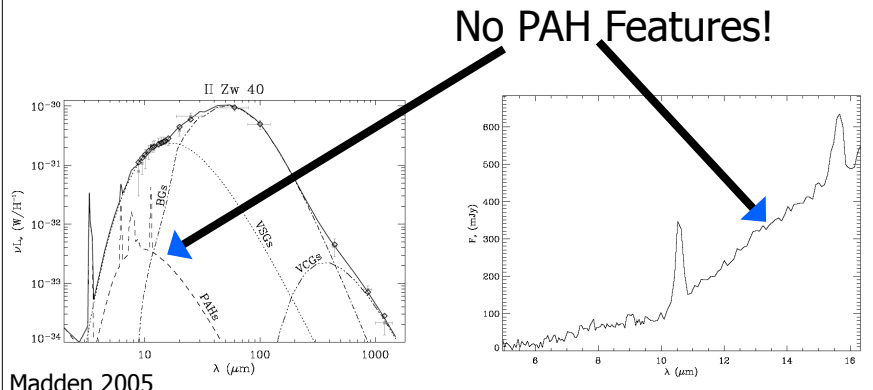
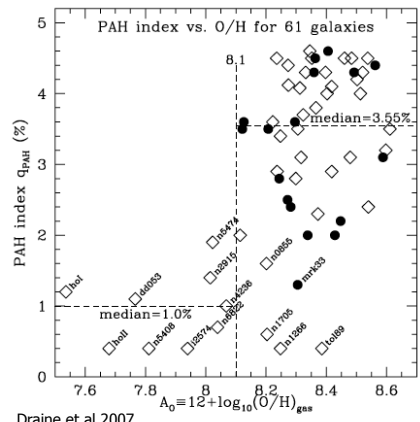


FIGURE 4. Examples of the MIR to mm observed data and modeled SED (left: [18]) and the MIR spectra for IIZw40 (right: [20]). Note the dearth of PAHs in the MIR spectra and the prominent [SIV] $\lambda 10.5\mu\text{m}$  and the [NeIII] $\lambda 15.5\mu\text{m}$  lines.

(data from Galliano et al 2005)

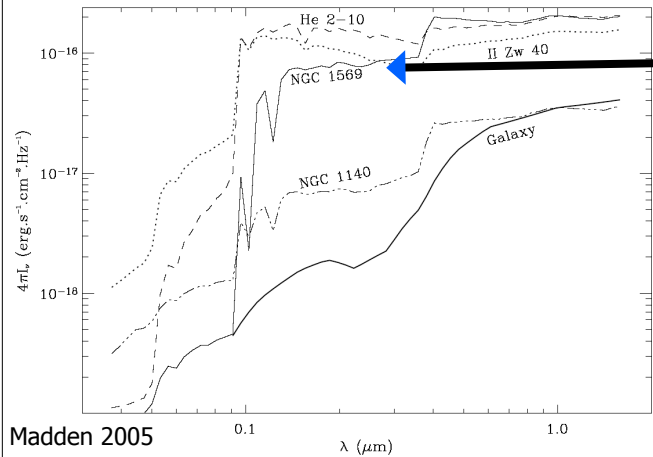
# Empirically, few PAH's in low metallicity galaxies

Madden et al 2006  
Wu et al 2006



Draine et al 2007  
Fig. 21.—PAH index (percentage of dust mass contributed by PAHs with  $N_C < 10^3$  C atoms) vs. galaxy metallicity (see text). Low-metallicity galaxies always have low PAH index  $q_{\text{PAH}}$ . Filled circles are SINGS-SCUBA galaxies; diamonds are SINGS galaxies lacking submillimeter data. [See the electronic edition of the *Journal for a color version of this figure.*]

# Example of harder radiation fields in low metallicity dwarfs



Harder = more UV

FIGURE 5. Examples of the variations of the modeled ISRFs for 4 of the dwarf galaxies, compared to the softer ISRF of the Galaxy.